

## Anisotropic Velocity Imaging of Saturated Sandstone under Laboratory True Triaxial Stress State Using Ultrasonic Surveys

*M. GhofraniTabari, S.D. Goodfellow, M.H.B Nasser, and R. P. Young*

*Lassonde Institute, University of Toronto*

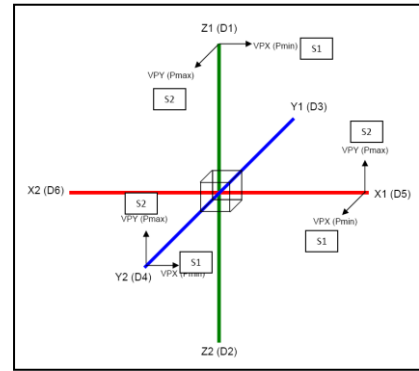
### Summary

Investigating the anisotropic models in water saturated sandstone specimens at different stages of loading under true triaxial stress regime during the experiment with drained conditions, gives an idea about anisotropy models of rock under in situ stress regimes in different depths in mines, or in the oil, gas, and geothermal fields for the sake of operation designs such as excavation, hydraulic fracturing or hydrocarbon exploration. A polyaxial or true triaxial test (TTT) conducted on cubes of Fontainebleau sandstone in Prof. R Paul Young's Rock Fracture Dynamics Facility (RFDF) laboratory at Lassonde Institute, provided an opportunity to test our modelling techniques. The True Triaxial Geophysical Imaging Cell (TTGIC) is armed with an ultrasonic and acoustic emission monitoring system which can perform transducer to transducer ultrasonic velocity surveys to image anisotropic velocity structure of the sample during the experiment. Due to the existence of several loading boundary effects especially edge effects and friction between surfaces of the platen and the rock specimen, loaded stress is not uniformly distributed in the specimen. Hence, ellipsoidal anisotropy occurs along with distributed heterogeneities as compaction and lower-stressed zones are introduced in the rock by closure and opening of the pre-existing cracks. Therefore, a numerical simulation using FLAC3D on the non-uniform distribution of stress in the specimen as well as shear wave splitting analysis is utilized to estimate the compaction boundary pseudo-surfaces within the rock. Anisotropic velocity images of the rock sample with evolving P- and S-wave velocities along the orthogonal principal directions under various polyaxial stress states are obtained and discussed. Moreover, isotropic elastic media, when triaxially stressed, constitute a special sub-set of orthorhombic media, called ellipsoidal media which can be used as a default velocity model for active P-wave tomography of the specimen. Once the acoustic emission activity increases after the crack closure and compaction period, distribution of stress-aligned fluid-filled microcracks creates extensive-dilatancy anisotropy which alters the elastic properties in different directions. Dilatancy is associated with acoustic emission, increase of volumetric strain and permeability, and decrease of ultrasonic wave velocities. Hence, a barrier property of the solid rock known as dilatancy boundary criterion can be defined transitioning from the compaction boundaries in the polyaxial experiment which separates areas with dilatant and nondilatant behaviors.

### Geophysical Imaging Cell and Experiment Setup

A state of the art True-Triaxial Geophysical Imaging Cell (TTGIC) designed and manufactured by ErgoTech Company is used at the Rock Fracture Dynamic Facility (RFDF) laboratory at University of Toronto under supervision of Prof. R. Paul Young to study rock fracture physics under three-dimensional polyaxial compressive stress regime. A Fontainebleau sandstone cubic sample was prepared using a Wasino CNC grinding machine with an accuracy of 5 micron flatness on each face. After being placed in the True Triaxial Geophysical Imaging Cell (TTGIC), they went under an evolving loading pattern exerted by the MTS machine. The Fontainebleau specimen was tested first at hydrostatic stress of 5 MPa. Then, the loading pattern moved on to a true-triaxial loading state with a stress ratio ( $\sigma_2/\sigma_3=7$ ) where,  $\sigma_3$  and  $\sigma_2$  were kept at a constant stress of 5 and 35 MPa respectively during the experiment. In the meanwhile,  $\sigma_1$  gradually increased up to the failure of the rock at 490 MPa. In this experiment,  $\sigma_3$  and  $\sigma_2$  were applied under load control mode on two paired horizontal actuators (along  $X=\sigma_3$  and  $Y=\sigma_2$  directions) while simultaneously

maintaining a constant load on two opposite sides of the cubic specimen. However,  $\sigma_1$  (along Z or vertical direction) was raised under a constant displacement control rate of 0.0002 mm/s up to failure (Nasseri et al, 2014). Using an integrated pulser/amplifier system software, the ultrasonic wave velocity survey measured compressional ( $V_P$ ) and two shear wave velocities ( $V_{S1}$  and  $V_{S2}$ ) along all three principal stress directions at various stages of loading in a set of directions and polarizations shown above.



### Simulation of Stress Distribution with FLAC3D

Estimated physical parameters of the sandstone sample are used to simulate the stress distribution in FLAC3D shown in figure below. Following the stress evolution pattern that the rock went through during the experiment, the loads were numerically applied at the end of each platen in FLAC3D for different stages of the test. Also, stereonet representations of apparent P-wave velocities are obtained from transducer to transducer velocity surveys at different stages of the experiment.

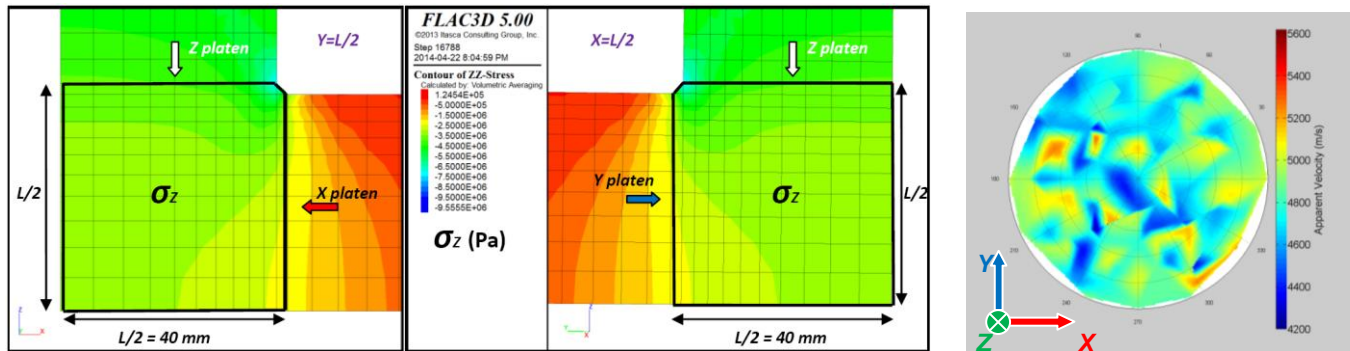
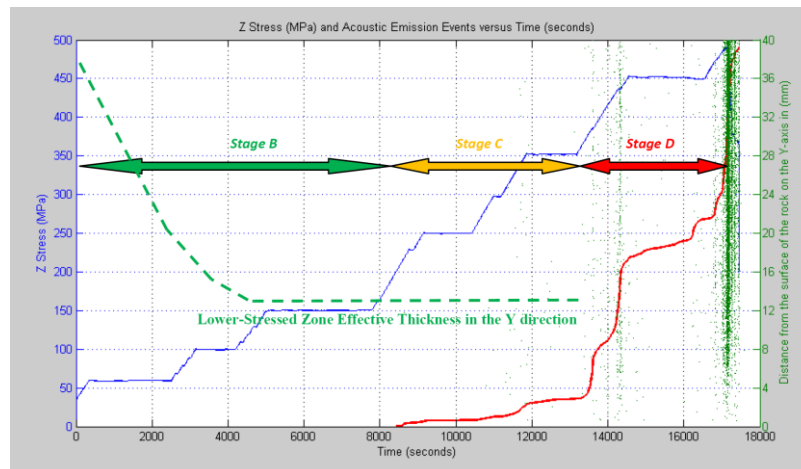


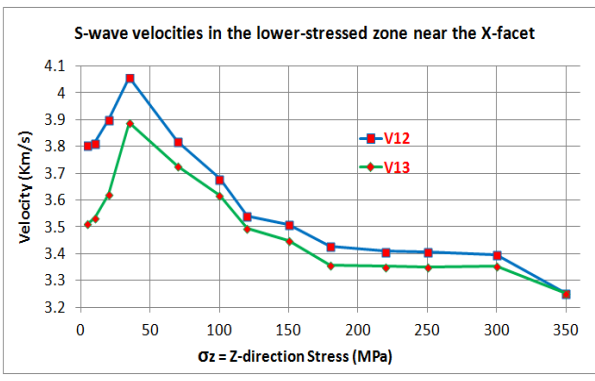
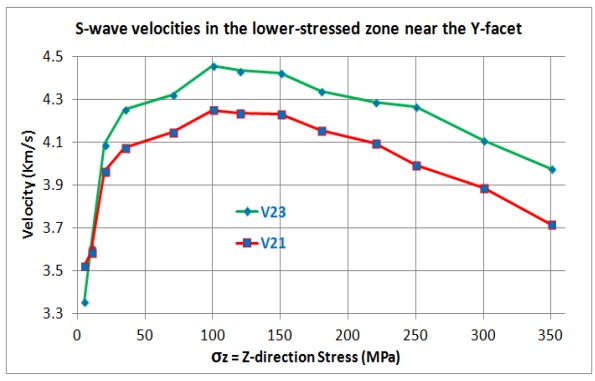
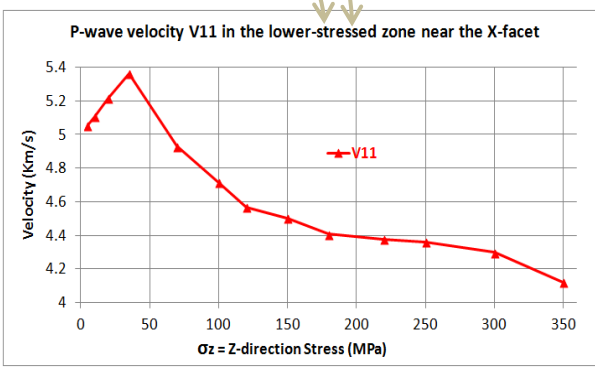
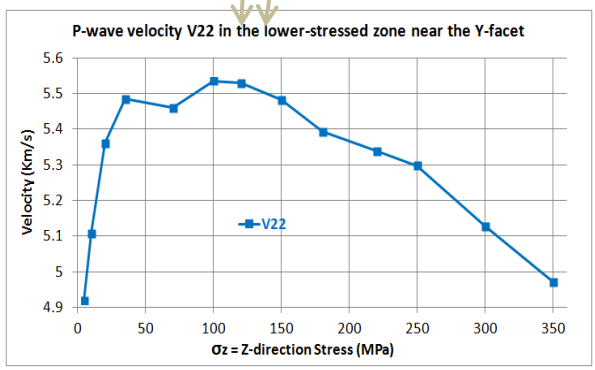
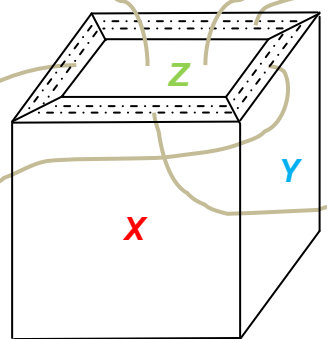
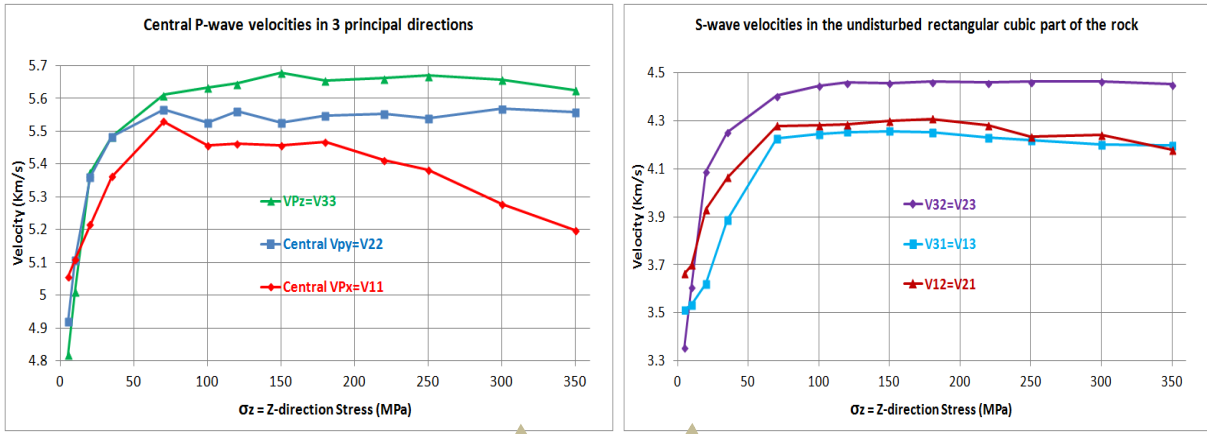
Figure below shows the main principal stress evolution (blue line), cumulative acoustic emission activity (red line) and distance of the AE events distributed between the center of the rock and the surfaces in the minimum principal stress direction (green dots). The experiment was divided by different stages based on phase shifts in compaction or dilation of the rock.



The compaction pseudo-boundary (or lower-stressed zone effective thickness) shown with dashed line in figure above as well as the one in the intermediate principal stress direction, are used in calculating the P and S wave velocities in different domains introduced in the rock under polyaxial stress state.

### Velocity Structure of the Cubic Rock under True Triaxial Stress State

Figure below shows a schematic view of the rock with its central compacted domain and four lower-stressed domains near the X and Y facets divided by compaction pseudo-boundaries along with their corresponding resolved shear and compressional wave velocity values under polyaxial stress state.



### Stiffness Tensor Parameters

In the coordinate system associated with the symmetry planes (i.e., each coordinate plane is a plane of symmetry), orthorhombic media have 9 independent stiffness components within its symmetrical stiffness matrix,

$$c^{(ort)} = \begin{bmatrix} c_{11} & c_{12} & c_{13} & 0 & 0 & 0 \\ c_{21} & c_{22} & c_{23} & 0 & 0 & 0 \\ c_{31} & c_{32} & c_{33} & 0 & 0 & 0 \\ 0 & 0 & 0 & c_{44} & 0 & 0 \\ 0 & 0 & 0 & 0 & c_{55} & 0 \\ 0 & 0 & 0 & 0 & 0 & c_{66} \end{bmatrix}$$

within which the diagonal components can be directly obtained by P and S wave velocities as shown in the following equations. There are also different methods to solve for the off-diagonal stiffness matrix components. Cheadle et al [1991] have solved them for Orthorhombic media. However, there are two other approaches for calculation of the off-diagonal coefficients based on ellipsoidal anisotropy symmetry. The first approach known as Rudzki's ellipticity conditions for ellipsoidal anisotropy (Helbig, 1983 and, Rasolofosaon, 1998) is based upon the assumption that the magnitude of the components of the stress deviator is small compared to the wave moduli (eg. stiffness coefficient). It derives a relationship between the stiffness coefficients and the three principal stresses. The second approach derived by Daley et al [2006] constructs eikonal equations using the standard linearized approximation of the phase velocity for quasi-compressional (qP) wave propagation in a weakly anisotropic orthorhombic medium. Both methods suggest a degenerate (ellipsoidal) case of qP wave propagation in an orthorhombic medium with an ellipsoidal slowness surface. They derive equations to obtain the three off-diagonal stiffness coefficients from the other 6 independent diagonal stiffness matrix components. All the three abovementioned methods were examined and solutions were provided and compared with each other. The dimensionless Thomsen parameters (Thomsen, 1986) which characterize the anisotropy of a medium are industry standard and is used in many commercial software. We used the relationship of generic Thomsen parameters for a medium with ellipsoidal anisotropy provided by Tsvankin [1997] shown in table below to calculate anisotropy parameters of our specimen.

$$\left\{ \begin{array}{l} c_{11} = \rho V_{11}^2 \\ c_{22} = \rho V_{22}^2 \\ c_{33} = \rho V_{33}^2 \\ c_{44} = \rho V_{23}^2 = \rho V_{32}^2 \\ c_{55} = \rho V_{13}^2 = \rho V_{31}^2 \\ c_{66} = \rho V_{21}^2 = \rho V_{12}^2 \end{array} \right.$$

Thomsen Parameter	$\epsilon$	$\gamma$	$\delta$
y-z plane	$\epsilon^{(1)} = \frac{c_{22} - c_{33}}{2c_{33}}$	$\frac{c_{66} - c_{55}}{2c_{55}}$	$\frac{(c_{23} + c_{44})^2 - (c_{33} - c_{44})^2}{2c_{33}(c_{33} - c_{44})}$
x-z plane	$\epsilon^{(2)} = \frac{c_{11} - c_{33}}{2c_{33}}$	$\frac{c_{66} - c_{44}}{2c_{44}}$	$\frac{(c_{13} + c_{55})^2 - (c_{33} - c_{55})^2}{2c_{33}(c_{33} - c_{55})}$
x-y plane	$\epsilon^{(3)} = \frac{c_{22} - c_{11}}{2c_{11}}$	$\frac{c_{55} - c_{44}}{2c_{44}}$	$\frac{(c_{12} + c_{66})^2 - (c_{11} - c_{66})^2}{2c_{11}(c_{11} - c_{66})}$

## Conclusions

Time-lapse ultrasonic velocity imaging of the rock was provided along with an anisotropic symmetry analysis of the rock by calculating the stiffness tensor parameters. The polyaxial experiment procedure on Fontainebleau sandstone cubic specimen is described and information about the Geophysical Imaging Cell and laboratory setup are provided. The experiment was divided to four different stages based on the shift in behavior of physical parameters representing the micro-crack properties of the rock. The physical parameters were acquired through different measurements including stress, strain, and P, S1, and S2 wave velocities along the three principal axes, and transducer to transducer velocity surveys are explained and demonstrated. Then, numerical simulations of time-lapse stress distribution in the cubic sample are accomplished by using FLAC3D software. Also, stereonet representations of directional velocity evolution were obtained by mapping the P-wave apparent velocities on stereograms. Compaction boundary pseudo-surfaces are estimated by stress distribution analysis along the minimum and intermediate principal axes to calculate the time-lapse evolution of shear and P-wave velocities in the intact and lower-stressed domains of the rock. Different velocity domains of the cubic rock are displayed in a schematic view. Thereafter, diagonal and off-diagonal stiffness tensor parameters were derived and compared based on different theories for ellipsoidal and orthorhombic medium. Finally, Thomsen's parameters are calculated to give a sense about the anisotropy strength in the rock.

## Acknowledgements

I would like to acknowledge Laszlo Lombos who put a lot of effort in manufacturing our geophysical imaging cell (TTGIC) in the Ergotech Company. Also, I acknowledge Hamed OwladeGhaffari for his helpful scientific comments.

## References

- Backus, G. E. (1965). Possible forms of seismic anisotropy of the uppermost mantle under oceans. *Journal of Geophysical Research*, 70(14), 3429-3439.
- Berryman, J. G., Grechka, V. Y., & Berge, P. A. (1999). Analysis of Thomsen parameters for finely layered VTI media. *Geophysical Prospecting*, 47(6), 959-978.
- Berryman, J. G. (2007). Seismic waves in rocks with fluids and fractures. *Geophysical Journal International*, 171(2), 954-974.
- Charalampidou, E. M. (2011). Experimental study of localised deformation in porous sandstones (Doctoral dissertation, Heriot-Watt University).
- Chaudhry N.A. (1995). Effects of aligned discontinuities on the elastic and transport properties of reservoir rocks. PhD thesis, University of London.
- Cheadle, S. P., Brown, R. J., & Lawton, D. C. (1991). Orthorhombic anisotropy: A physical seismic modeling study. *Geophysics*, 56(10), 1603-1613.
- Crampin, S., & McGonigle, R. (1981). The variation of delays in stress-induced anisotropic polarization anomalies. *Geophysical Journal of the Royal Astronomical Society*, 64(1), 115-131.
- Crampin, S. (1984). An introduction to wave propagation in anisotropic media. *Geophysical Journal International*, 76(1), 17-28.
- Crampin, S. (1987). Geological and industrial implications of extensive-dilatancy anisotropy. *Nature*, 328, 491-496.
- Crampin, S., & Peacock, S. (2005). A review of shear-wave splitting in the compliant crack-critical anisotropic Earth. *Wave Motion*, 41(1), 59-77.
- Every, A. G., & Sachse, W. (1992). Sensitivity of inversion algorithms for recovering elastic constants of anisotropic solids from longitudinal wavespeed data. *Ultrasonics*, 30(1), 43-48.
- Fjar, E., Holt, R. M., Raaen, A. M., Risnes, R., & Horsrud, P. (2008). *Petroleum related rock mechanics* (Vol. 53). Elsevier.
- Grechka, V., Singh, P., & Das, I. (2011). Estimation of effective anisotropy simultaneously with locations of microseismic events. *Geophysics*, 76(6), WC143-WC155.
- Haimson, B., & Chang, C. (2000). A new true triaxial cell for testing mechanical properties of rock, and its use to determine rock strength and deformability of Westerly granite. *International Journal of Rock Mechanics and Mining Sciences*, 37(1), 285-296.
- Helbig, K. (1983). Elliptical anisotropy-its significance and meaning. *Geophysics*, 48(7), 825-832.
- Helbig, K. (1993). Longitudinal directions in media of arbitrary anisotropy. *Geophysics*, 58(5), 680-691.
- Helbig K. (1994). Foundations of anisotropy for exploration seismics. *Handbook of Geophysical Exploration*, 22, Pergamon, Oxford UK.
- Helbig, K., & Thomsen, L. (2005). 75-plus years of anisotropy in exploration and reservoir seismics: A historical review of concepts and methods. *Geophysics*, 70(6), 9ND-23ND.
- Johnson, P. A., & Rasolofosaon, P. N. J. (1996). Nonlinear elasticity and stress-induced anisotropy in rock. *Journal of Geophysical Research: Solid Earth* (1978–2012), 101(B1), 3113-3124.
- King, M. S., Chaudhry, N. A., & Shakeel, A. (1995, February). Experimental ultrasonic velocities and permeability for sandstones with aligned cracks. In *International journal of rock mechanics and mining sciences & geomechanics abstracts* (Vol. 32, No. 2, pp. 155-163). Pergamon.
- King, M. S., Shakeel, A., & Chaudhry, N. A. (1997). Acoustic wave propagation and permeability in sandstones with systems of aligned cracks. *Geological Society, London, Special Publications*, 122(1), 69-85.
- King, M. S. (2002). Elastic wave propagation in and permeability for rocks with multiple parallel fractures. *International journal of rock mechanics and mining sciences*, 39(8), 1033-1043.
- King, A., & Talebi, S. (2007). Anisotropy effects on microseismic event location. *Pure and Applied Geophysics*, 164(11), 2141-2156.
- King, M. S. (2009). Recent developments in seismic rock physics. *International Journal of Rock Mechanics and Mining Sciences*, 46(8), 1341-1348.
- King, M. S., Pettitt, W. S., Haycox, J. R., & Young, R. P. (2012). Acoustic emissions associated with the formation of fracture sets in sandstone under polyaxial stress conditions. *Geophysical Prospecting*, 60(1), 93-102.
- Lombos, L., Roberts, D. W., & King, M. S. (2012). Design and Development of Integrated True Triaxial Rock Testing System. *True Triaxial Testing of Rocks*, 35. (Proceedings of the TTT Workshop, held in Beijing, Oct. 17 2011).
- Mahmoudian, F., Margrave, G. F., Daley, P. F., & Wong, J. (2010). Determining elastic constants of an orthorhombic material by physical seismic modeling. *A A*, 22(2), 2.
- Mahmoudian, F., Margrave, G. F., Daley, P. F., Wong, J., & Henley D. C. (2014). Estimation of elastic stiffness coefficients of an orthorhombic physical model using group velocity analysis on transmission data. *Geophysics*, v. 79, p. R27-R39
- Marion, D., Mukerji, T., & Mavko, G. (1994). Scale effects on velocity dispersion: From ray to effective medium theories in stratified media. *Geophysics*, 59(10), 1613-1619.
- Maxwell, S. C., & Young, R. P. (1992). Sequential velocity imaging and microseismic monitoring of mining-induced stress change. *pure and applied geophysics*, 139(3-4), 421-447.
- Maxwell, S. C., & Young, R. P. (1993). Associations between temporal velocity changes and induced seismicity. *Geophysical research letters*, 20(24), 2929-2932.
- Maxwell, S. C., & Young, R. P. (1995). A controlled in-situ investigation of the relationship between stress, velocity and induced seismicity. *Geophysical research letters*, 22(9), 1049-1052.
- Maxwell, S. C., & Young, R. P. (1996, October). Seismic imaging of rock mass responses to excavation. In *International journal of rock mechanics and mining sciences & geomechanics abstracts* (Vol. 33, No. 7, pp. 713-724). Pergamon.

- Mensch, T., & Rasolofosaon, P. (1997). Elastic-wave velocities in anisotropic media of arbitrary symmetry—generalization of Thomsen's parameters  $\epsilon$ ,  $\delta$  and  $\gamma$ . *Geophysical Journal International*, 128(1), 43-64.
- Mogi, K. (1967). Effect of the intermediate principal stress on rock failure. *Journal of Geophysical Research*, 72(20), 5117-5131.
- Mogi, K. (1971). Fracture and flow of rocks under high triaxial compression. *Journal of Geophysical Research*, 76(5), 1255-1269.
- Mogi, K. (1977). Dilatancy of rocks under general triaxial stress states with special reference to earthquake precursors. *Journal of Physics of the Earth*, 25(Supplement), S203-S217.
- Mogi, K. (2007). *Experimental rock mechanics*. CRC Press.
- Mukerji, T., & Mavko, G. (1994). Pore fluid effects on seismic velocity in anisotropic rocks. *Geophysics*, 59(2), 233-244.
- Nasseri, M. H. B., Goodfellow, S.D., Young, R. P., & Lombos, L. (2014) 3-D transport and acoustic properties of Fontainebleau sandstone during true-triaxial deformation experiments, *International Journal of Rock Mechanics and Mining Sciences*, Volume 69, July 2014, Pages 1-18
- Nur, A., & Simmons, G. (1969). Stress-induced velocity anisotropy in rock: An experimental study. *Journal of Geophysical Research*, 74(27), 6667-6674.
- Nur, A. (1971). Effects of stress on velocity anisotropy in rocks with cracks. *Journal of Geophysical Research*, 76(8), 2022-2034.
- O'Connell, R. J., & Budiansky, B. (1974). Seismic velocities in dry and saturated cracked solids. *Journal of Geophysical Research*, 79(35), 5412-5426.
- Pettitt, W. S., & King, M. S. (2004). Acoustic emission and velocities associated with the formation of sets of parallel fractures in sandstones. *International Journal of Rock Mechanics and Mining Sciences*, 41, 151-156.
- Popp, T., & Salzer, K. (2007). Anisotropy of seismic and mechanical properties of Opalinus clay during triaxial deformation in a multi-anvil apparatus. *Physics and Chemistry of the Earth, Parts A/B/C*, 32(8), 879-888.
- Rasolofosaon, P. (1998). Stress-induced seismic anisotropy revisited. *Oil & Gas Science and Technology*, 53(5), 679-692.
- Rudzki, M. P. (1911). Parametrische Darstellung der elastischen Welle in anisotropen Medien: Anzeiger der Akademie der Wissenschaften Krakau. Imprimerie de l'Université. p. 503-536.
- Sarkar, D., Bakulin, A., & Kranz, R. L. (2003). Anisotropic inversion of seismic data for stressed media: Theory and a physical modeling study on Berea Sandstone. *Geophysics*, 68(2), 690-704.
- Sayers, C. M. (1988). Inversion of ultrasonic wave velocity measurements to obtain the microcrack orientation distribution function in rocks. *Ultrasonics*, 26(2), 73-77.
- Sayers, C. M., Van Munster, J. G., & King, M. S. (1990, October). Stress-induced ultrasonic anisotropy in Berea sandstone. In *International Journal of Rock Mechanics and Mining Sciences & Geomechanics Abstracts* (Vol. 27, No. 5, pp. 429-436).
- Sayers, C. M., & Munster, J. G. (1991). Microcrack-induced seismic anisotropy of sedimentary rocks. *Journal of Geophysical Research: Solid Earth* (1978–2012), 96(B10), 16529-16
- Sayers, C. M. (2002). Stress-dependent elastic anisotropy of sandstones. *Geophysical prospecting*, 50(1), 85-95.
- Schoenberg, M., & Sayers, C. M. (1995). Seismic anisotropy of fractured rock. *Geophysics*, 60(1), 204-211.
- Schoenberg, M., & Helbig, K. (1997). Orthorhombic media: Modeling elastic wave behavior in a vertically fractured earth. *Geophysics*, 62(6), 1954-1974.
- Shakeel, A., & King, M. S. (1998). Acoustic wave anisotropy in sandstones with systems of aligned cracks. *Geological Society, London, Special Publications*, 136(1), 173-183.
- Shearer, P. M. (1999). *Introduction to seismology*. Cambridge University Press.
- Shi, L., Li, X., Bai, B., Li, Q., & Feng, X. (2012). Numerical analysis of loading boundary effects in Mogi-type true triaxial tests. *True Triaxial Testing of Rocks*, 19.
- Tao, G., & King, M. S. (1990, October). Shear-wave velocity and Q anisotropy in rocks: A laboratory study. In *International Journal of Rock Mechanics and Mining Sciences & Geomechanics Abstracts* (Vol. 27, No. 5, pp. 353-361). Pergamon.
- Thomsen, L. (1986). Weak elastic anisotropy. *Geophysics*, 51(10), 1954-1966.
- Tsvankin, I. (1997). Anisotropic parameters and P-wave velocity for orthorhombic media. *Geophysics*, 62(4), 1292-1309.
- Tsvankin, I. (2001). Seismic signatures and analysis of reflection coefficients in anisotropic media. *Handbook of Geophysical Exploration*, Volume 29
- Tsvankin, I., Gaiser, J., Grechka, V., van der Baan, M., & Thomsen, L. (2010). Seismic anisotropy in exploration and reservoir characterization: An overview. *Geophysics*, 75(5), 75A15-75A29.
- Young, R. P., Hutchins, D. A., McGaughey, J., Towers, J., Jansen, D., & Bostock, M. (1989) (I). Geotomographic imaging in the study of mining induced seismicity. pure and applied geophysics, 129(3-4), 571-596.
- Young, R. P., Hutchins, D. A., Talebi, S., Chow, T., Falls, S., Farrell, L., Jansen, D., McGaughey, J., Towers, J., & Urbancic, T. (1989). Laboratory and field investigations of rockburst phenomena using concurrent geotomographic imaging and acoustic emission/microseismic techniques. pure and applied geophysics, 129(3-4), 647-659.
- Young, R. P., & Maxwell, S. C. (1992). Seismic characterization of a highly stressed rock mass using tomographic imaging and induced seismicity. *Journal of Geophysical Research: Solid Earth* (1978–2012), 97(B9), 12361-12373.
- Young, R. P., Nasseri, M. H. B., & Lombos, L. (2012). Imaging the Effect of the Intermediate Principal Stress on Strength, Deformation and Transport Properties of Rocks Using Seismic Methods. *True Triaxial Testing of Rocks*, 4, 167.